ACS APPLIED MATERIALS & INTERFACES

Research Article

www.acsami.org

Topotactic Growth, Selective Adsorption, and Adsorption-Driven Photocatalysis of Protonated Layered Titanate Nanosheets

Qili Wu,[†] Xianfeng Yang,[§] Jia Liu,[†] Xin Nie,[‡] Yongliang Huang,[†] Yuping Wen,[†] Javid Khan,[†] Wasim U. Khan,[†] Mingmei Wu,*[,†] and Taicheng An*[,‡]

[†]MOE Key Laboratory of Bioinorganic and Synthetic Chemistry, State Key Laboratory of Optoelectronic Materials and Technology, Key Laboratory of Environment and Energy Chemistry of Guangdong Higher Education Institutes, School of Chemistry and Chemical Engineering, Sun Yat-Sen (Zhongshan) University, Guangzhou 510275, P. R. China

[‡]State Key Laboratory of Organic Geochemistry and Guangdong Key Laboratory of Environmental Resources Utilization and Protection, Guangzhou Institute of Geochemistry, Chinese Academy of Sciences, Guangzhou 510640, P. R. China

[§]Institute of Bioengineering and Nanotechnology, 31 Biopolis Way, the Nanos, #04-01, 138669 Singapore

Supporting Information

ABSTRACT: Layered titanates with selective adsorption ability and adsorption-driven photocatalytic property can be quite attractive due to their potential applications in water purification. In this work, lepidocrocite-like layered protonated titanate ($H_2Ti_2O_5·H_2O$, denoted as HTO) nanosheets were successfully synthesized by an ion-exchange process. It turns out that this layered structure displays an abundant and selective adsorption toward the fluoroquinolone pharmaceutical compared with some large dye molecules due to a size selectivity of the interlayer spacing of HTO and the molecular horizontal size, as well as their electrostatic interaction. The uptake ability of HTO could be readily controlled through adjusting the pH values of adsorbate solution, and the maximum uptake capacity was achieved at the pH value of about 5.5 for ciprofloxacin (CIP) and 6.5 for moxifloxacin (MOX). The adsorption amount of smaller nalidixic acid (NAL) showed an increasing tendency as the pH value decreased. Moreover, the two-dimensional layered crystal structure also permits such HTO nanosheets to have a large percentage of (010) faces exposed, which is considerably provided by the interlayer surfaces of these nanosheets. The (010) surface has a similar Ti and O atomic arrangement as to the highly reactive anatase TiO_2(001) one. Due to these specific characteristics, these HTO nanosheets show excellent photocatalytic activity in degrading CIP under UV light irradiation as well as possess a superior adsorption ability to remove CIP from aqueous solution selectively and efficiently. The photocatalytic reaction is believed to be mainly conducted on the active anatase (001)-like interlayer (010) surfaces of the layered structures since the as-prepared HTO performs an adsorption-driven molecular recognitive photocatalytic reaction.

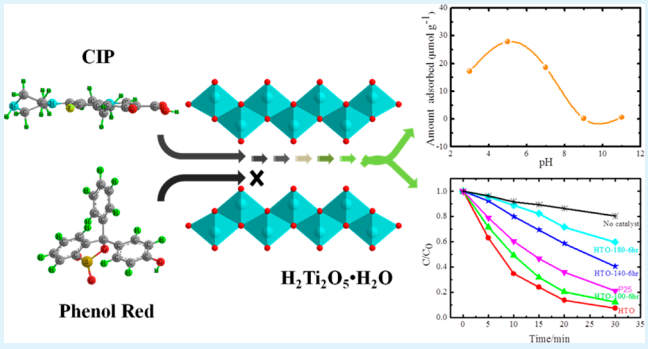

KEYWORDS: *layered titanate, selective adsorption, adsorption-driven photocatalysis, ciprofloxacin, anatase (001)-like surface*

1. INTRODUCTION

Zeolite-like molecular recoginitive adsorption and efficient photocatalysis has been an attractive approach with its great superiority to decompose a targeted pollutant in the environment.[1−3] In most cases, it is difficult for one photocatalyst to remove all pollutants in one system.[4] While in the system containing mixed organic pollutants, the photocatalyst will generally degrade high-level pollutants first via a free-radical oxidation, resulting in that the target pollutants will not be removed efficiently.[5] Therefore, selective adsorption and photocatalysis for degradation of a targeted pollutant among the mixture turns quite meaningful. To achieve this, an ideal material should have highly selective adsorption for a targeted organic molecule and possess excellent photocatalytic activity. Many efforts have been devoted to inherent framework structure design and outer crystal surface modification to optimize the access for targeted molecules to reach the active sites readily. Among the efforts, quite a lot of strategies such as surface charge, magnetism, porosity, and even electronic band structure modifications have been applied to realize molecular recognition for photocatalysis selectively and efficiently.[6,7] However, meticulous, rigorous, and complex chemical approaches are generally required for these surface decorations, for example, the molecule imprinting and surfactant templating to create magnetic adsorbent[8] and porous shell,[9] respectively.

Received: June 27, 2014
Accepted: September 18, 2014
Published: September 18, 2014

 © 2014 American Chemical Society

Layered titanates with an abundant interlayer surface have been widely used in ion-exchange, adsorption, and catalysis due to their unique two-dimensional crystal structures and excellent chemical activity.[10−14] Generally, an ion-exchange process between interlayer ions of the layered titanates and ions in solution has been carried out for the purpose to either remove target ions from the solution or obtain a new layered material.[15−18] For instance, layered titanates ($Na_2Ti_3O_7 \cdot nH_2O$) with exchangeable sodium cations were used to adsorb target cations (e.g., Sr^{2+}, Ba^{2+}, Ag^+, and Cu^{2+}, etc.) from water.[16,19] However, successful achievements about layered titanates with molecular-specific adsorption and corresponding adsorption-driven photocatalytic reaction are limited. With few examples in this field, Makoto Ogawa and his co-workers have made a great contribution.[20−22] They modified a layered titanate, i.e., $K_{0.8}Ti_{1.73}Li_{0.27}O_4$ (KTLO), by silylation with two different organic functional units (alkyl and phenyl groups) through a dodecyltrimethylammonium-exchanged form as the intermediate. The interlayer functioned titanate could be used to adsorb 4-nonylphenol (NPh) selectively and efficiently.[22] The attached organic molecules inside the interface could be decomposed upon UV light irradiation. They also modified KTLO inside the interlayer space with iron oxide on a molecular level through a reaction between KTLO and an Fe(III) acetylacetonate complex.[20] The composite material was found to be an excellent catalyst for oxidation of cyclohexane under sunlight irradiation with highly selective, up to 100% production of cyclohexanone and cyclohexanol. The interlayer space with a suitable gallery height may lead to a prompt desorption to prevent successive oxidation of cyclohexanone and cyclohexanol.[20] In addition, layered sodium titanates ($M_xTi_{2-x/3}Li_{x/3}O_4$; M = Na^+) derived from KTLO in an aqueous NaOH solution containing propylamine could selectively adsorb benzene in a mixed aqueous solution of benzene, phenol, and 4-butylphenol due to a size-exclusive and zeolite-like effect.[21] Subsequently, the adsorbed benzene could be decomposed inside the sodium titanate upon UV irradiation. Both $M_xTi_{2-x/3}Li_{x/3}O_4$ (M = K^+) and $M_xTi_{2-x/3}Li_{x/3}O_4$ (M = Li^+) could not work. This was primarily attributed to that the distance of the adjacent titanate sheets in water for $Na_xTi_{2-x/3}Li_{x/3}O_4$ (x = 0.61) is the largest among the tree titanates, and the benzene molecule with its size of 0.6 × 0.6 × 0.3 nm^3 is smaller than the interface space with a gallery height of 0.7 nm.[21] However, why can these layered titanates show obvious photocatalytic activity after the adsorption? In the last five years, growing enthusiasm has been dedicated to the outer facet structure of a crystal on its catalysis, typically photocatalysis.[23,24] Herein for the photocatalysis of these titanates, we are convinced that the inner interlayer surface structure should play a key role in the efficient photocatalysis.

Ciprofloxacin (CIP) is a typical fluoroquinolone antimicrobial, used as a broad-spectrum antibacterial agent, and has a large consumption every year.[25] Many cases have been reported about its presence and pollution due to hospital effluent and unfriendly discard.[26,27] Typically in some places, CIP concentration in wastewater and even surface water has been up to several hundred nanograms/liter. The detections of some wastewater in Switzerland sewage sludge showed that the concentration of CIP could be in the range from 1.40 to 2.42 mg/kg. Although studies have shown that CIP may be adsorbed into sediments or photodegraded, it has been stated in some documents that there is a high risk for its pollution, and it is necessary to employ a treatment process to destroy the residual CIP molecules in aqueous environment. Therefore, it is of great importance to find an ideal material to selectively remove CIP and/or related species from environmental water and consequently decompose it/them efficiently.[28−30]

Recently, the growth, nanostructure, adsorption, and catalysis of protonated titanate nanotubes and nanosheets have been receiving considerable attention.[31−33] However, layered protonated titanates combining dual functions of excellent adsorption and adsorption-driven photocatalysis have not been achieved because in most cases the protonated titanates display relatively weaker exchange ability than alkali ones as mentioned previously.[34] Just recently in this Journal, Wong and Lu reported that layered protonated titanate nanosheets were used as absorbents of methylene blue and Pb^{2+}.[32] In this paper, we have synthesized the protonated titanate simply and made a great achievement in its ion exchange directly with organic molecules. The layered hydrogen titanium oxide hydrate (HTO) nanosheets were synthesized by a simple topotactic ion-exchange process from the $K_xTi_{2-x/3}Li_{x/3}O_4$ (x = 0.8) precursor in aqueous solution of hydrochloric acid. The as-synthesized HTO without any additional modification by either inorganic or organic species inside the interlayer has molecular selective adsorption ability and photocatalytic activity to fluoroquinolones as compared to other larger organic molecules (for example, phenol red (PR)). The molecular recognitive adsorption ability is attributed to perfect match of both space sizes and charges between the HTO interlayer and fluoroquinolone molecules. The adsorption ability could be controlled by pH values of fluoroquinolone solution, and the maximum uptake capacity was obtained at a pH value of about 5.5 and 6.5 for CIP and MOX (moxifloxacin), respectively. The adsorption capacity of NAL (nalidixic acid) increased as the pH value reduced. Therefore, the as-synthesized HTO sample is believed to have pH-dependent adsorption to fluoroquinolone molecules and can be used as a favorable adsorbent to fluoroquinolone molecules. In addition, HTO showed excellent photocatalytic activity compared with commercial P25 when CIP was employed as a model of the organic pollutant under UV light irradiation. The efficient photocatalytic reaction is believed to be an adsorption-driven process based on the two-dimensional layered crystal structure and a large percentage of anatase (001)-analogy active interlayer (010) surfaces.

2. EXPERIMENTAL SECTION

The titanium n-tetrabutoxide ($[Ti(OC_4H_9)_4]$, TNB) was chemically pure, and all others were analytically pure. Ciprofloxacin (CIP) was purchased from Sigma-Aldrich (>98% purity). All of these reagents were used without further purification.

2.1. Synthesis of the Precursor Alkali Titanate Nanosheet. As prepared in Yang's work,[35] $K_xTi_{2-x/3}Li_{x/3}O_4$ (KTLO, x = 0.8) nanosheets were synthesized by dropwise addition of TNB to aqueous lithium hydroxide (LiOH) solution at room temperature under vigorous stirring for about 15 min. Then potassium hydroxide (KOH) solution was added to the mixture as a mineralization reagent. After that, the reaction system was transferred into a Teflon-lined autoclave for hydrothermal treatment at 180 °C for 24 h. The KTLO white precipitate was obtained by centrifugation and then washed with distilled water and alcohol several times to thoroughly clean it; afterward, it was dried at 60 °C.

2.2. Hydrothermal Treatment of the KTLO Precursor in HCl Solution. An amount of 0.156 g of as-prepared KTLO (about 1.5 mmol of Ti) was loaded into a Teflon-lined autoclave containing 15 mL of hydrochloric acid (0.05 mol L^{-1}) for hydrothermal treatment at a predetermined temperature between 100 and 180 °C for different

times. The resultant products were separated by centrifugation, washed with distilled water, and dried at 60 °C.

2.3. Characterization. Powder X-ray diffraction (XRD) was taken on a Rigaku D/max diffraction system with a Cu K_α source. A scanning electron micrograph (SEM) was obtained using a FEI Quanta scanning electron microscope operated at 20 kV. The transmission electron microscopy (TEM) was performed on a JEOL JEM-2010 transmission electron microscope operated at 200 kV. An UV−vis−NIR spectrophotometer (UV-3150) was used to get the absorption spectrum. Thermogravimetric analysis (TGA) was conducted on a TG209 thermogravimetry. BET surface areas of samples were analyzed using an Automated vapor sorption analyzer (Autosorb-iQ2-MP (Quanta Chrome)) at 77.4 K under vacuum. An UV-2450 spectrophotometer was chosen to obtain UV−vis diffuse reflectance spectra of those products using $BaSO_4$ as the reference sample. Zeta potentials are obtained on a nanoparticle size−zeta potential and molecular weight analyzer (EliteSizer, Brookhaven). A Rietveld refinement method was used to quantify the percentage of each component in a sample with mixture phases.

2.4. Adsorption and Photocatalysis. An amount of 0.15 g of the as-synthesized sample was added into a Pyrex tube containing 150 mL of CIP solution at concentration of 54 μmol L^{-1} (20 mg L^{-1}). The tube has a double-walled cooling water jacket which could keep the solution temperature constant at about 25 °C throughout the experiment. The adsorption process was conducted in the dark with vigorous stirring. After every 10 min, 3.0 mL of reaction solution was extracted and filtered through Millipore filters with 0.22 μm, and then the filtered liquor was analyzed by HPLC.

When testing these samples for photocatalytic ability, UV light was turned on after adsorption for 40 min. The light source using a high-pressure mercury lamp (GGZ-125, Shanghai Yaming Lighting, E_{max} = 365 nm) with a power consumption of 125 W was located in the photocatalytic reactor side. The light intensity was about 0.7 mW cm^{-2} at the surface of the tube. Similarly, samples from the reaction solution (3 mL) were extracted at fixed intervals and filtered through 0.22 μm Millipore filters. All experiments were carried out at room temperature.

Adsorption and photocatalytic reactions of the other organic molecules (MOX, NAL, and phenol red (PR)) at different pH were conducted in the same way. The concentration of residual substrates in the supernatant was analyzed by using an UV−vis−NIR spectrophotometer.

The adsorption isotherms of CIP, MOX, and NAL were determined by equilibrating the HTO sample (10 mg) in each adsorbate solution of different pH values (10 mL, concentration varying from 0.0 to 136 μmol L^{-1}, corresponding to CIP concentration from 0.0 to 50 mg L^{-1}, pH ranging from 3.0 to 11) for 24 h at room temperature. Then an UV−vis−NIR spectrophotometer (UV-3150) was used to test the concentration of residua adsobates in the supernatant.

2.5. HPLC Analysis. The reaction solution after photocatalytic degradation was analyzed by an Agilent 1200 series HPLC with a Phenomenex Gemini C18 column, 250 mm × 4.6 mm i.d. The mobile phase, acetonitrile/water mixed solution (20:80, V/V) containing 20 mmol of phosphoric acid and 2.5 mmol of 1-heptanesulfonic acid sodium salt, was set at 1.0 mL min^{-1} with the column temperature of 30 °C, and the detection wavelength was fixed at 274 nm.[36]

3. RESULTS AND DISCUSSION

3.1. Growth and Thermal Stability of the Layered Protonated Titanate. The precursor, orthorhombic $K_xTi_{2-x/3}Li_{x/3}O_4$ (denoted as KTLO), is confirmed by a powder X-ray diffraction (XRD) pattern (JCPDS card No. 25-1353, a = 3.821 Å, b = 15.591 Å, c = 2.973 Å) (Figure S1a, Supporting Information). It crystallizes as nanosheets with a thickness of about 100 nm and two-dimensional size of about 600 nm × 1000 nm (Figure S1b−d, Supporting Information). The hydrothermal treatment of KTLO in HCl aqueous solution (0.05 mol) at 100 °C for 2 h results in pure orthorhombic hydrogen titanium oxide hydrate, $H_2Ti_2O_5{\cdot}H_2O$ (a = 3.784 Å, b = 18.03 Å, c = 2.998 Å) with an interlayer space expansion along the b-axis (Figure 1a1 and Figure S1a,

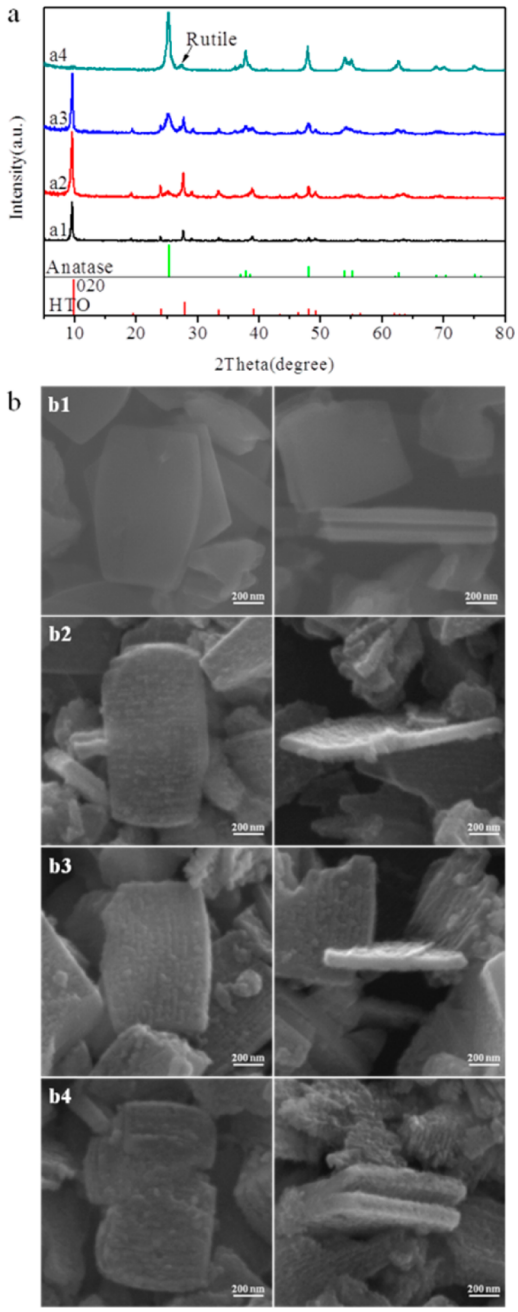

Figure 1. (a) XRD patterns and (b) SEM images with a top and side view of a typical nanosheet in each sample collected after KTLO precursor treated with 0.05 M HCl aqueous solution at different reaction conditions. (a1, b1) 100 °C for 2 h, (a2, b2) 100 °C for 6 h, (a3, b3) 140 °C for 6 h, and (a4, b4) 180 °C for 6 h. JCPDS No. 21-1272 for anatase and JCPDS No. 47-0124 for hydrogen titanium oxide hydrate, $H_2Ti_2O_5{\cdot}H_2O$ (HTO).

Supporting Information), while both a- and c-axis lengths have a negligible change.[34,35] As both the layered structure and plated shape (Figure S1b−d and 1b1, Supporting Information) can be preserved, this process can be regarded as a typical topotactic ion-exchange process.[10,19,22,34,35] When the precursor KTLO is mixed with dilute hydrochloric acid under stirring, K^+ ions can be replaced by H_3O^+ ones, and as a result the

interlayer space swells along the *b*-axis.[37] The presence of water molecules inside HTO is confirmed by thermogravimetric analysis (Figure S2a, Supporting Information). On heating up to 50 °C in air, a small quantity of adsorbed water molecules is lost without destruction of the layered structure (Figure S2b, Supporting Information). However, as it is heated to 100 °C with more loss of water molecules, the interlayer spacing shrinks (Figure S2b, Supporting Information), and the X-ray diffraction peaks related to the layered structure tend to be much weaker, suggesting an important electrostatic interaction between positively charged water molecules and negatively charged $(TiO_6)_n$ octahedral slabs to stabilize the layered HTO structure. The positively charged H_3O^+ ions have been intercalated among $(TiO_6)_n$ octahedral slabs during ion exchange with K^+ ions.[38,39] The release of the water molecules can take place at temperatures as low as around 100 °C in air, suggesting that the interaction between water molecules and $(TiO_6)_n$ octahedral slabs should not be as strong as the covalent coordination bond, and there is a possibility of hydrogen bonds between the intercalated water molecules and $(TiO_6)_n$ octahedral slabs.[10,40,41]

3.2. Adsorption of CIP by HTO. The protonated layered titanates, i.e., HTO nanosheets, display unique ability to adsorb organic molecules. With the coexistence of HTO and CIP in aqueous solution, the uptake of CIP molecules by HTO nanosheets can be achieved. The concentration of CIP in aqueous solution was found to decrease during stirring with the coexistence of HTO nanosheets (Figure 2a). The uptake of CIP was up to about 65% in the stock of HTO after 1 h of stirring. After the adsorption of CIP, the solution is analyzed by HPLC (Figure 2b). The HPLC results show only the CIP molecules present in the mother solution even after 40 min adsorption (Figure 2b3), indicating no new chemicals have been yielded and only adsorption has happened in this process. However, after 40 min of adsorption and followed by 15 min of photocatalysis under UV light, several additional HPLC peaks identified as degradation products can be detected from the aqueous solution (Figure 2b4). Therefore, the degradation reactions of the aqueous solution occur only under the UV irradiation.

When the precursory sample, i.e., KTLO, is hydrothermally treated in dilute hydrochloric acid at 100 °C for 6 h, a trace of anatase TiO_2 appears (Figure 1a2 and 1b2 and Figure S3b, Supporting Information). The resultant sample (denoted as HTO-100-6 h) with major of HTO nanosheets and 8.65% anatase nanoparticles (Figure 1b2 and Figure S3b, Supporting Information) also exhibit good adsorption ability, but not as good as the pure HTO does (Figures 2c1 and 2c2). Compared with the pure HTO sample, the sample with mixture phases suffers from a certain extent of destruction of the layered structure in HTO (Figure 1a2 and 1b2), and consequently its adsorption ability reduces (Figure 2c2). A sample obtained at higher temperature such as at 140 °C for 6 h (denoted as HTO-140-6 h), with more anatase (21.37%) emerging as nanoteeth arrays on the broad surface of HTO nanosheets in its possession (Figure 1a3 and 1b3 and Figure S3c, Supporting Information), shows much less adsorption ability toward CIP (Figure 2c3) due to its larger portion of anatase and worse destruction of the HTO layer structure. With further treatment in dilute HCl aqueous solution at higher temperature such as 180 °C for 6 h (denoted as HTO-180-6 h), KTLO nanosheets completely converted into TiO_2 nanocrystal arrays with trace rutile (Figure 1a4). 92.46% anatase nanocrystals and 7.54%

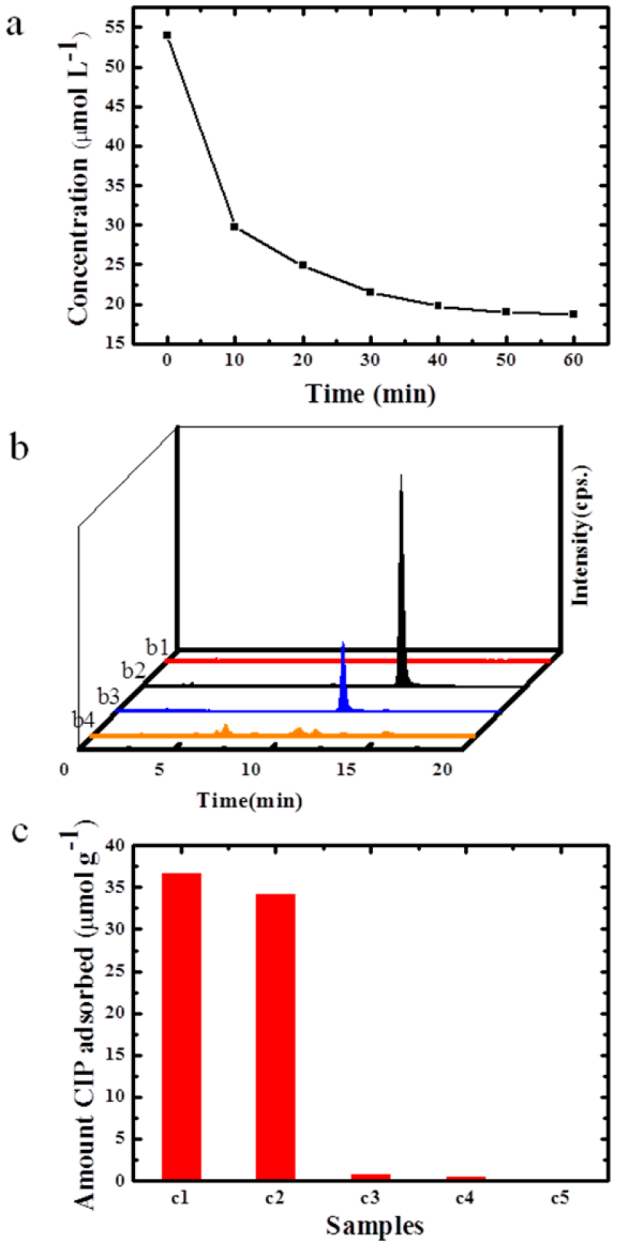

Figure 2. (a) CIP solution concentration at different adsoprtion time using HTO (2 h, 100 °C) as adsorbent at about pH 6. (b) HPLC chromatogram of the CIP solution during adsorption and photocatalysis reaction of HTO (2 h, 100 °C) (b1: deionized water, b2: original CIP solution without any treatment, b3: CIP solution after 40 min adsorption, b4: CIP solution after 40 min adsorption followed by 15 min photocatalysis). (c) The adsorbed amount of CIP molecules on the as-synthesized samples (c1: 100 °C for 2 h, c2: 100 °C for 6 h, c3: 140 °C for 6 h, c4: 180 °C for 6 h).

rutile covering the entire nanosheet are yielded (Figure 1a4 and 1b4 and Figure S3d, Supporting Information). At this moment, the uptake of CIP is negligible (Figure 2c4). Moreover, BET surface analysis shows that the surface areas of pure HTO, HTO-100-6 h, HTO-140-6 h, and HTO-180-6 h are 35, 52, 77, and 83 m^2/g, respectively. Surface areas increase as the single-crystal HTO nanosheet breaks to be a TiO_2 nanoparticles assembled nanosheet. However, the adsorption ability of these samples is not enhanced with the increasing surface areas. These experimental results confirmedly suggest the high adsorption ability for CIP is attributed to the two-dimensional

dx.doi.org/10.1021/am5041847 | ACS Appl. Mater. Interfaces 2014, 6, 17730−17739

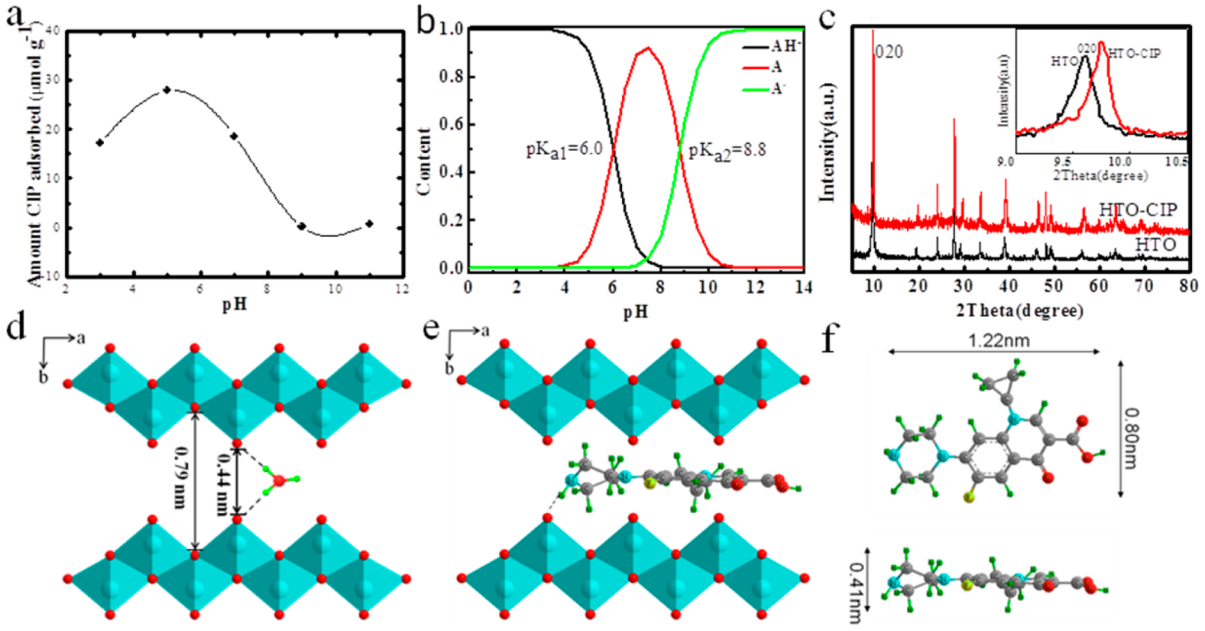

Figure 3. (a) Effect of pH values on HTO (2 h, 100 °C) adsorption performance toward CIP (C_0 = 54 μmol L^{-1}, 20 mg L^{-1}). (b) Its speciation at different pH values. (c) XRD patterns of HTO and its CIP-adsorbed sample (marked as HTO−CIP). Inset: the enlargement of the $(020)_H$ diffraction peak. Adsorption experiment was conducted at pH 6. (d) Schematic illustration of TiO_6 zigzag octahedral layers, interlayer H_3O^+, and H-bonding formed by the two parts in HTO crystal structure. (e) Illustration showing the possible situation of CIP molecule intercalating into the interspace of TiO_6 octahedral slabs. (f) CIP molecular structure from CSD (Cambridge Structural Database).

layered structure of HTO with intercalated positively charged water molecules but not to the three-dimensional dense framework structure of either anatase or rutile TiO_2 even with much higher surface areas.

3.3. pH-Dependent Adsorption. Adsorption characteristics are usually greatly influenced by the solution pH since most organic pollutants have ionizable functional groups at different pH.[42−44] Therefore, controlled adsorption will be realized by pH adjustment. The uptake of CIP by HTO is highly pH-dependent as observed in Figure 3a. The uptake amount of CIP initially increases with the increasing pH value and reaches a maximum at about pH 5.5 and then decreases at higher pH values. The observed adsorption behavior can be attributed to the pH-dependent character of CIP (Figure 3b). CIP molecular charge varies with pH value as its pK_{a1} = 6.0 and pK_{a2} = 8.8, respectively (Figure 3b).[45] The molecule is usually positively charged in acidic and negatively charged in basic aqueous solution. All the HTO samples have negative zeta potentials at about −10 to −20 mV when dispersed in neutral water. The relatively lower absolute zeta potentials were caused by the larger sizes of these HTO samples which could not be dispersed stably in water without any assistant dispersant. However, the TiO_6 octahedral slabs in titanates are usually considered as a negatively charged framework to keep charge balance with the interlayer cations.[39] Under weak acidic condition, CIP molecules positively charged can well match with negatively charged TiO_6 octahedral slabs in charge. It has been mentioned previously that the adsorption ability of soils to CIP in aqueous solution from acidic to neutral conditions is strongly dependent on the cation exchange capacity (CEC).[46] The best efficiency for capturing CIP at lower pH value should be attributed to the positively charged CIP molecules intercalating into the interlayer space of the titanate with replacing H_3O^+ and interacting with the negatively charged slabs in both charge and size match. This kind of interaction can lead to a minor change of the interlayer spacing. Actually, after the exchange of CIP molecules with water ones inside the interlayers, the 020 *d*-spacing tends to be smaller, suggesting the shrinking of the interlayer spacing (Figure 3c, inset).

As for the layered HTO nanosheet, its layered structure is topotactic converted from a KTLO layered structure, with crystal water and H_3O^+ in the interlayer. The most possible arrangement of the interlayer H_3O^+ ions is added in Figure 3d. According to Sasaki and Feng's work,[38,47] this stacking mode of $(TiO_6)_n$ octahedral slabs makes surface oxygen atoms in the adjacent layers face each other and produces pseudocubic cavities in the interlayer gallery. The H_3O^+ ions should be located in these cavities, and one cavity accommodates one H_3O^+. Because $(TiO_6)_n$ octahedral slabs are negatively charged, they need to be neutralized by H^+. Therefore, the two H^+ in H_3O^+ will direct to the surface oxygen atoms in each side of the $(TiO_6)_n$ octahedral slabs in the form of hydrogen bonds (Figure 3d). Crystal structure analysis shows that the minimum interlayer distance between two TiO_6 octahedral layers is about 0.44 nm (Figure 3d), which is quite suitable for one CIP molecule intercalating horizontally (Figure 3e). A CIP molecule is about 1.22 nm long, 0.80 nm wide, and 0.41 nm thick (Figure 3f).[48] The maximum interlayer distance is about 0.79 nm, and consequently hydrogen bonding is expected between the intercalary CIP molecules and the TiO_6 octahedral slabs, which will lead to a relatively stronger interaction between the CIP molecules and layer frameworks. The powder XRD results in Figure 3c indicate that the 020 *d*-value of HTO (marked as HTO−CIP in Figure 3c, inset) shrinks a little as compared to that of the pristine HTO after capturing CIP molecules. This is the result of a stronger interaction between positively charged CIP molecules and negatively charged TiO_6 octahedral slabs. A similar phenomenon has been identified in Yang's work in which they used layer-structured $Na_2Ti_3O_7$ nanofibers to

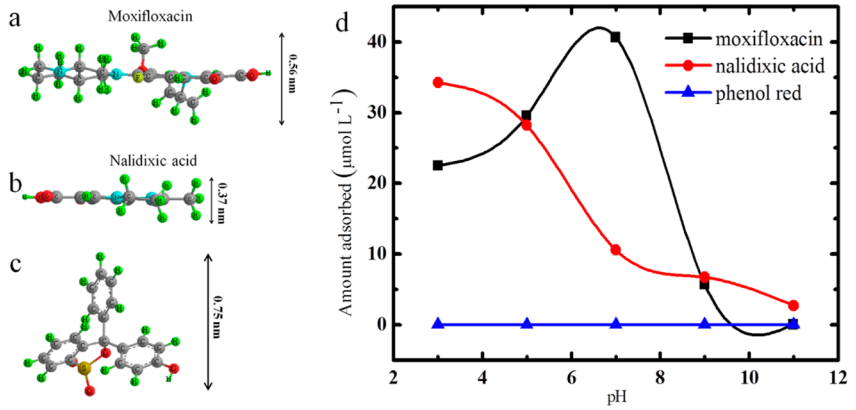

Figure 4. (a–c) Side view of moxifloxacin, nalidixic acid, and phenol red molecular structures from CSD (Cambridge Structural Database). (d) pH-dependent adsorption of HTO to these three adsorbates (C_0 = 54 μmol L^{-1}).

conduct an ion exchange between Na^+ and either Sr^{2+} or Ba^{2+} in aqueous solution.[19]

To further confirm the pH-dependent selective adsorption ability of the HTO sample, two more fluoroquinolone molecules which share a similar molecular skeleton with CIP were chosen to be adsorbates. The first one is MOX with a molecule size of 1.43 nm long, 0.85 nm wide, and 0.56 nm high (Figure 4a), and the second one is NAL with a molecule size of 1.00 nm long, 0.78 nm wide, and 0.37 nm high (Figure 4b).[49−51] Since the lateral size of the MOX molecule is 0.56 nm, larger than the HTO interlayer space, it is supposed it will not be readily absorbed at first sight. However, it has been reported that, in chemical environments, the negatively charged $Ti_xO_y^{n-}$ layer on the side underneath the surface will be neutralized by H^+ cations. The Ti−O bond contraction on the top surface will happen to some degree when releasing a surface hydrogen atom. If the average number of hydrogen loss becomes large enough, the surface layer of HTO can be stripped.[52] Figure S4a (Supporting Information) compares the dry HTO and wet HTO samples after soaking in water of different pH (3, 7, and 11) for 24 h. It shows clearly that wet HTO samples have larger $d_{(020)}$-spacing than dry HTO. What is more, expansion of interlayer spacing increases as solution pH value decreased from 11 to 3. Therefore, it is believed that the interlayer space of HTO may have a slight expansion when dispersed in water, which makes adsorption of MOX possible. The adsorption capacity of HTO for MOX reached the highest value at a pH value around 7 and decreased as the solution turns to be acidic. HTO showed negligible adsorption of MOX in alkaline solution. As for NAL, a much smaller molecule compared with CIP (Figure 4c), an increasing adsorption behavior was observed from pH 11 to pH 3 (Figure 4d, the red curve). Generally, adsorption of ionizable organic contaminants is affected by pH due to the varied species. The species distributions of CIP, MAX, and NAL as a function of pH are depicted in Figure 3b and Figures S4b and S4c (Supporting Information). The different adsorption behavior of HTO to these three adsorbates at different pH values has a close relationship with molecule speciation at different pH values. The pKa1 and pKa2 of MOX are 5.7 and 9.4, respectively, while those of CIP are 6.0 and 8.8 as well as those of NAL 4.8 and 5.9. The maximal distribution for zwitterionic MOX, CIP, and NAL species is around pH values of 7.5, 7.1, and 5.3, respectively (Figure 3b and Figures S4b and S4c, Supporting Information). XRD and SEM of HTO after adsorbing MOX and NAL are shown in Figure S4d–f (Supporting Information). Like that of HTO after adsorbing CIP, XRD of HTO after adsorbing MOX in Figure S4d (Supporting Information) also shows a slight right-shift of peak $(020)_H$. Therefore, MOX molecules must be adsorbed into the interlayer space of HTO like what happened to CIP molecules. Therefore, it is possible there is a strong interaction between MOX and $(TiO_6)_n$ octahedral slabs. The d-value of $(020)_H$ after adsorbing NAL shows no change compared with $d(020)$ of the original HTO sample. This could be attributed to weaker interaction of the intercalated adsorbates and $(TiO_6)_n$ octahedral slabs. Among the three fluoroquinolones, the NAL molecule has the smallest size, and it will have a certain space for movement in the interlayer spacing, which leads to a loose bonding between NAL and the $(TiO_6)_n$ octahedral slabs. SEM in Figures S4e and S4f (Supporting Information) presents that the HTO nanosheet structure maintained nearly changeable after adsorption, indicating a good stability of this structure.

The adsorption isotherms of HTO to these three adsorbates in different pH solution were investigated separately (Figure S5, Supporting Information). The Langmuir model and Freundlich model, the most accepted surface adsorption models for single solute systems, were chosen to fit these adsorption data, but neither one matched. Some other adsorption models like Harkins–Jura, Jovanovic, and Tempkin also failed to fit these data. This may be caused by the specific size-selective-intercalation and charge-interaction adsorption mechanism of HTO nanosheets to these fluoroquinolones, which makes it improper to use those existing adsorption models to describe the HTO adsorption process. In addition, adsorption isotherms in Figure S5 (Supporting Information) show that adsorption capacities of HTO to all these three adsorbates are greatly influenced by the pH value of the solution. In general, the acidic environment is much more favored in the adsorption than basic solution. The experiment data also show that the maximum adsorption capacities for these three adsorbates could be obtained when the original adsorbate concentration is more than 81 μmol L^{-1} (corresponding to 30 mg L^{-1} of CIP solution). Maximum adsorption capacities of HTO to CIP, MOX, and NAL were about 40 μmol g^{-1} at pH 5, 55 μmol g^{-1} at pH 7, and 40 μmol g^{-1} at pH 3, respectively.

3.4. Selective Adsorption Ability. The protonated layered titanate (HTO) shows high selective adsorption ability. Besides the pH value dependent adsorption ability, layered HTO nanosheets with a specific interlayer space could act as a

selective adsorbent like those zeolite materials. Only molecules with acceptable sizes and matched charges could be adsorbed by the as-synthesized HTO samples. To prove this, the adsorption behavior of HTO to a three-dimensional molecule (Phenol Red, PR) with relatively larger sizes (1.02 nm × 0.97 nm × 0.75 nm, Figure 4c) was investigated.[53] Results came out just like predicted. The HTO sample showed no adsorption ability to PR throughout all the pH range (Figure 4d, blue curve). Since NAL, CIP, and MOX are typical fluoroquinolone molecules with smaller, middle, and lager size, respectively, the as-synthesized HTO sample is believed to have attractive adsorption ability toward almost all the fluoroquinolones. Meanwhile, the adsorption behavior of each molecule could also be adjusted by controlling the solution pH values. Therefore, a specific molecule will be adsorbed preferentially if its favored adsorption pH is used. This study proves that layered protonated titanates can also be potentially promising adsorbents for some pharmaceuticals with molecular recognition and opens up a new window for searching new selective adsorbents for pharmaceutical delivery.

3.5. Enhanced Photocatalysis. The photocatalytic activity of HTO and other related samples converted from KTLO was comparatively investigated with an identical concentration of CIP solution (0.54 μmol L^{-1}) as shown in Figure 5. Pure HTO

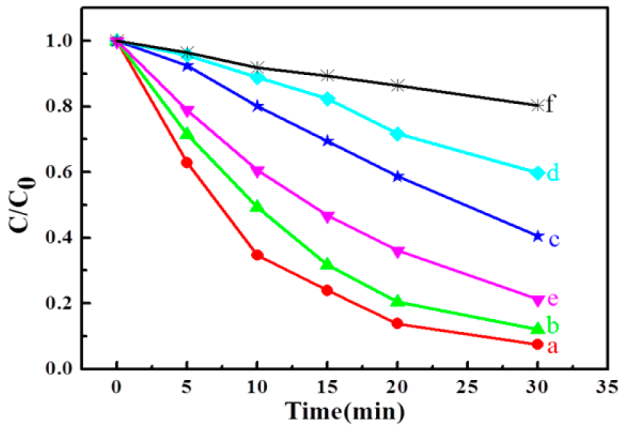

Figure 5. Photocatalytic degradation of CIP by different as-prepared products (a–d), Degussa P25 (e), and no catalyst (f). (a–d) represent the products obtained by treating KTLO with 0.05 M HCl aqueous solution at (a) 100 °C for 2 h, (b) 100 °C for 6 h, (c) 140 °C for 6 h, and (d) 180 °C for 6 h, respectively.

shows the best photocatalytic efficiency, even much better than commercial catalyst P25 (Degussa). With the growth of teeth-like anatase nanocrystal arrays on the broad surfaces of the HTO platelets (Figure 1b), the photocatalytic efficiency declines, which indicates a higher photocatalytic activity of HTO nanosheets than that of anatase nanocrystals. Diffuse reflection spectra of these samples in Figure S6 (Supporting Information) presents that all these samples have UV light adsorption ability, and their absorption edges exhibit a systematic blue shift with increasing amount of TiO_2. According to previous reports, the band gaps of anatase and rutile are 3.2 and 3.0 eV, respectively.[54] As for pure HTO ($H_2Ti_2O_5{\cdot}H_2O$) in this work, the optical bandgap (E_g) can be obtained by the classical Tauc equation[55]

$$\alpha h\nu = A(h\nu - E_g)^n$$

in which α, ν, A, and E_g represent the absorption coefficient, light frequency, proportionality constant, and bandgap, respectively. As for n, it determines the characteristics of the transition in a semiconductor; the value is 1/2 for a direct and 2 for an indirect optical transition. Data analysis shows that the band gap of HTO is indirect. As a result, HTO is calculated to have a band gap of 3.44 eV. It has been confirmed that the HTO nanosheet is a single crystal which is constructed by $(TiO_6)_n$ slabs layer by layer along the b-axis leading to a large percentage of (010) facets exposed (Figure S7a and S7b, Supporting Information). According to the TEM images in Figure S7c (Supporting Information), the anatase particles growing on the HTO substrate choose to expose (101) facets due to the lower surface energy of these planes, combined with a trace percentage of active (001) surfaces. It has been well established in general that the photocatalysis of a crystal is dependent on the surface structure and surface activity of the crystal facets.[24,40,56,57] These TiO_2 nanocrystals will perform a lower efficiency in the photocatalytic degradation as compared with those with (001) facets exposed. The growth of anatase nanocrystals takes place on the broad (010) surfaces of HTO (Figure 1b2–4). The more anatase TiO_2 nanocrystals form, the less HTO will exist followed by a decrease of the $(010)_H$ (subscript H denoted as HTO) facets exposed. It is confidently believed that $(010)_H$ surface atomic arrangement of HTO is significantly related to the efficiencies of the photocatalysis.

HTO can be definitely obtained via treating KTLO with proper acids by ion exchange and can inherit the layered TiO_6 octahedral framework structure from KTLO (Figure 1b and Figure S3, Supporting Information).[35,47,58] The configuration of TiO_6 octahedral slabs on and perpendicular to $(010)_H$ facets is shown in Scheme 1. From a detailed analysis of the crystal

Scheme 1. Comparison of Atomic Arrangement between HTO (Top) and Anatase (Bottom) on (001) and (010) Planes (Represented by Bars and Balls on the Left Panel) As Well As on (010) and (001) Planes (Represented by Octahedra on the Right Panel), Respectively[a]

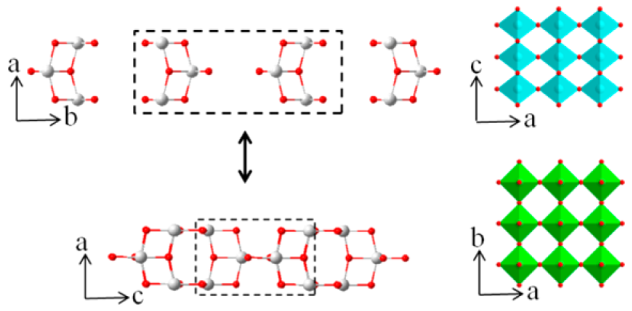

[a]Red balls for O and gray balls for Ti atoms. For an obvious comparison, the interlayer spacing in HTO is in an arbitrary ratio.

structure between HTO and anatase, it can be found that the atomic arrangement of oxygen and titanium on the $(010)_H$ surface is quite similar to that on $(001)_A$ (subscript A denoted as anatase). The view vertical to a (001) plane of HTO (Scheme 1) suggests that the configuration of the Ti–O bond fragment inside the dashed-lined rectangle is quite similar to that on the (010) one of anatase (Scheme 1). On the top-left panel in Scheme 1, each Ti_3O_7 fragment stands for one slab on the (010) plane of HTO with a top view along the c-axis, while on the bottom-left panel, each one stands for one (001) lattice

plane of anatase with a top view along the *b*-axis. The connection of TiO_6 octahedra on the (010) plane of HTO is similar to that on the (001) one of anatase TiO_2 (right panel). With a view along the ⟨010⟩ direction, the construction of Ti−O bonds of HTO likes slices of anatase along the ⟨001⟩ direction. It is addressed by Wu et al. that a delaminated nanosheet with lepidocrocite-like structure could demonstrate abundant anatase (001)-like surfaces.[41] They confirmed this demonstration based on their experimental results that such nanosheets performed an obvious dissociative adsorption process of water, which had been observed on the anatase (001) surface. Their thermogravimetric analysis (TGA) results indicated that, except for the desorption of adsorbed molecular water from ∼50 to ∼150 °C, these nanosheets also exhibited an additional weight dropoff at 350 °C which could be defined as the loss of hydroxyl groups. In our work, similar TG results of HTO nanosheets are observed in Figure S2a (Supporting Information). A quick weight drop can be observed from ∼50 to ∼100 °C which corresponds to the loss of adsorbed water molecules. Subsequently, a relatively slow weight loss is observed from ∼100 to ∼350 °C that corresponds to hydroxyl groups. On the basis of the crystal structure analysis and TG results of HTO, it can be suggested that the as-prepared HTO nanosheets have a similar performance on its (010) ones as anatase (001) facets do. That means the (010) facets of HTO have a similar high reactivity as the (001) facets of anatase TiO_2 do. Because of the high surface energy, anatase (001) facets will diminish quickly during crystal growth for the purpose to minimize the whole crystal's surface energy. As a result, most reported anatase TiO_2 crystals are usually dominated by (101) facets, while (001) facets exposed to anatase are seldom observed unless using some special methods like using HF solution as reported by Yang et al.[24,59] In this study, based on the topotactic conversion from KTLO precursory nanosheets to HTO ones, (010) facets dominated HTO nanosheets can readily be obtained. In addition, the as-synthesized HTO nanosheets have a significantly large percentage of (010) facets, especially the "inside" interlayer (010) surfaces due to its two-dimensional layered structure, which can considerably contribute to a high activity of this material in many relevant applications, such as photocatalysis. It is certain that the efficiencies of photocatalysis were observed to decrease with reduction in the percentages of HTO in the samples (Figure 5a−d). Figure S8 (Supporting Information) shows the XRD patterns and SEM image of HTO nanosheets recollected after photocatalysis reaction. No significant structure and morphology changes are observed, indicating a good stabilization of HTO sample during the adsorption and photocatalysis process.

Compared with photocatalytic efficiency of CIP in Figure 5, HTO shows negligible photocatalysis to a larger molecule PR. Therefore, another conclusion can be drawn that more adsorption will lead to more active photocatalysis.[60,61] In other words, the as-prepared HTO performs an adsorption-driven photocatalytic reaction. The photocatalytic reaction is believed to be able to conduct on the abundant interlayer (010) surface of the layered slabs with analogy (001) surface active of anatase.[22] Therefore, the amount of uptake affects the performance of photocatalytic degradation. All these results confirm that the as-synthesized HTO is not only a good selective adsorbent but also a superior photocatalyst for CIP and other related fluoroquinolones.

4. CONCLUSION

Layered HTO nanosheets combining highly selective adsorption ability with excellent photocatalytic activity toward CIP and related fluoroquinolone antimicrobial molecules under UV light irradiation were reported, which are superior to that of the commercial TiO_2−P25 material. The adsorption ability results from its interlayer space between two negatively charged TiO_6 octahedral slabs, which are perfectly suitable for a positively charged CIP molecule with a thickness of 0.41 nm to intercalate laterally in neutral or acid solution. The adsorbing capacity can be adjusted by changing the pH values of CIP solution, and it reaches the maximum at the pH of 5.5. The excellent photocatalytic property of this material is highly related to its adsorption property and largely exposed (010) planes which have a surface structure similar to the highly reactive anatase (001) ones. Therefore, the layered HTO nanosheets may become a superior photocatalyst with high selectivity due to its two-dimensional structure and abundant (010) interlayer surfaces. Such a concept should be applicable to many other layered materials. Since there are so many kinds of layered materials and each has its own specific interlayer space and chemical property, both molecular selective adsorption toward specific molecules and adsorption-driven photocatalysis will be expected. Therefore, the present research work will open up more new opportunities for molecular recognition and selectively removing pollutants.

■ ASSOCIATED CONTENT

Supporting Information

XRD patterns and SEM images of KTLO precursor; TG analysis of HTO and corresponding XRD patterns at RT, 50, and 100 °C; low-magnification SEM images of samples after acid treatment; XRD of HTO in different pH solution; XRD and SEM of HTO after adsorption or photocatalysis reaction, adsorption isotherms of HTO to CIP, MOX, NAL, and DRS of all the HTO samples; and TEM analysis of the HTO nanosheet. This material is available free of charge via the Internet at http://pubs.acs.org.

■ AUTHOR INFORMATION

Corresponding Authors

*E-mail: ceswmm@sysu.edu.cn (M.W.)
*E-mail: antc99@gig.ac.cn (T.A.).

Notes

The authors declare no competing financial interest.

■ ACKNOWLEDGMENTS

This work was financially supported by NSFC (21271190, 41373102, and 40973068), the Government of Guangdong Province for NSF (S2012020011113) and industry (2012B09000026), and the State Key Laboratory of Inorganic Synthesis and Preparative Chemistry, Jilin University (2012-01).

■ REFERENCES

(1) Fox, M. A.; Dulay, M. T. Heterogeneous Photocatalysis. *Chem. Rev.* **1993**, *93*, 341−357.
(2) Lazar, M. A.; Daoud, W. A. Achieving Selectivity in TiO_2-Based Photocatalysis. *RSC Adv.* **2013**, *3*, 4130−4140.
(3) Roy, P.; Dey, T.; Lee, K.; Kim, D.; Fabry, B.; Schmuki, P. Size-Selective Separation of Macromolecules by Nanochannel Titania Membrane with Self-Cleaning (Declogging) Ability. *J. Am. Chem. Soc.* **2010**, *132*, 7893−7895.

(4) Li, G.; Park, S.; Kang, D.-W.; Krajmalnik-Brown, R.; Rittmann, B. E. 2,4,5-Trichlorophenol Degradation Using a Novel TiO_2-Coated Biofilm Carrier: Roles of Adsorption, Photocatalysis, and Biodegradation. *Environ. Sci. Technol.* **2011**, *45*, 8359−8367.
(5) Inumaru, K.; Kasahara, T.; Yasui, M.; Yamanaka, S. Direct Nanocomposite of Crystalline TiO_2 Particles and Mesoporous Silica as a Molecular Selective and Highly Active Photocatalyst. *Chem. Commun.* **2005**, *16*, 2131−2133.
(6) Lazar, M. A.; Daoud, W. A. Selective Adsorption and Photocatalysis of Low-temperature Base-modified Anatase Nanocrystals. *RSC Adv.* **2012**, *2*, 447−452.
(7) Liang, S.; Liang, R.; Wen, L.; Yuan, R.; Wu, L.; Fu, X. Molecular Recognitive Photocatalytic Degradation of Various Cationic Pollutants by the Selective Adsorption on Visible Light-driven $SnNb_2O_6$ Nanosheet Photocatalyst. *Appl. Catal., B* **2012**, *125*, 103−110.
(8) Tang, H.; Zhu, L.; Yu, C.; Shen, X. Selective Photocatalysis Mediated by Magnetic Molecularly Imprinted Polymers. *Sep. Purif. Technol.* **2012**, *95*, 165−171.
(9) Shiraishi, Y.; Sugano, Y.; Inoue, D.; Hirai, T. Effect of Substrate Polarity on Photocatalytic Activity of Titanium Dioxide Particles Embedded in Mesoporous Silica. *J. Catal.* **2009**, *264*, 175−182.
(10) Britvin, S. N.; Lotnyk, A.; Kienle, L.; Krivovichev, S. V.; Depmeier, W. Layered Hydrazinium Titanate: Advanced Reductive Adsorbent and Chemical Toolkit for Design of Titanium Dioxide Nanomaterials. *J. Am. Chem. Soc.* **2011**, *133*, 9516−9525.
(11) Gunjakar, J. L.; Kim, T. W.; Kim, H. N.; Kim, I. Y.; Hwang, S. J. Mesoporous Layer-by-Layer Ordered Nanohybrids of Layered Double Hydroxide and Layered Metal Oxide: Highly Active Visible Light Photocatalysts with Improved Chemical Stability. *J. Am. Chem. Soc.* **2011**, *133*, 14998−15007.
(12) Shen, L.; Uchaker, E.; Zhang, X.; Cao, G. Hydrogenated $Li_4Ti_5O_{12}$ Nanowire Arrays for High Rate Lithium Ion Batteries. *Adv. Mater.* **2012**, *24*, 6502−6506.
(13) Song, Z. Q.; Xu, H. Y.; Li, K. W.; Wang, H.; Yan, H. J. Hydrothermal Synthesis and Photocatalytic Properties of Titanium Acid $H_2Ti_2O_5$ Center Dot-H_2O Nanosheets. *Mol. Catal. A-Chem.* **2005**, *239*, 87−91.
(14) Wang, Y.; Hong, Z.; Wei, M.; Xia, Y. Layered $H_2Ti_6O_{13}$-Nanowires: A New Promising Pseudocapacitive Material in Non-Aqueous Electrolyte. *Adv. Funct. Mater.* **2012**, *22*, 5185−5193.
(15) Ide, Y.; Matsuoka, M.; Ogawa, M. Efficient Visible-Light-Induced Photocatalytic Activity on Gold-Nanoparticle-Supported Layered Titanate. *J. Am. Chem. Soc.* **2010**, *132*, 16762−16764.
(16) Li, N.; Zhang, L.; Chen, Y.; Fang, M.; Zhang, J.; Wang, H. Highly Efficient, Irreversible and Selective Ion Exchange Property of Layered Titanate Nanostructures. *Adv. Funct. Mater.* **2012**, *22*, 835−841.
(17) Liu, W.; Wang, T.; Borthwick, A. G. L.; Wang, Y.; Yin, X.; Li, X.; Ni, J. Adsorption of Pb^{2+}, Cd^{2+}, Cu^{2+} and Cr^{3+} onto Titanate Nanotubes: Competition and Effect of Inorganic Ions. *Sci. Total Environ.* **2013**, *456−457*, 171−180.
(18) Xie, S. F.; Zheng, B. J.; Kuang, Q.; Wang, X.; Xie, Z. X.; Zheng, L. S. Synthesis of Layered Protonated Titanate Hierarchical Microspheres with Extremely Large Surface Area for Selective Adsorption of Organic Dyes. *CrystEngComm* **2012**, *14*, 7715−7720.
(19) Yang, D. J.; Zheng, Z. F.; Zhu, H. Y.; Liu, H. W.; Gao, X. P. Titanate Nanofibers as Intelligent Absorbents for the Removal of Radioactive Ions from Water. *Adv. Mater.* **2008**, *20*, 2777−2781.
(20) Hattori, H.; Ide, Y.; Ogo, S.; Inumaru, K.; Sadakane, M.; Sano, T. Efficient and Selective Photocatalytic Cyclohexane Oxidation on a Layered Titanate Modified with Iron Oxide under Sunlight and CO_2 Atmosphere. *ACS Catal.* **2012**, *2*, 1910−1915.
(21) Ide, Y.; Nakasato, Y.; Ogawa, M. Molecular Recognitive Photocatalysis Driven by the Selective Adsorption on Layered Titanates. *J. Am. Chem. Soc.* **2010**, *132*, 3601−3604.
(22) Ide, Y.; Ogawa, M. Interlayer Modification of a Layered Titanate with Two Kinds of Organic Functional Units for Molecule-Specific Adsorption. *Angew. Chem., Int. Ed.* **2007**, *119*, 8601−8603.
(23) Liu, G.; Yang, H. G.; Pan, J.; Yang, Y. Q.; Lu, G. Q.; Cheng, H.-M. Titanium Dioxide Crystals with Tailored Facets. *Chem. Rev.* **2014**, DOI: 10.1021/cr400621z.
(24) Yang, H. G.; Sun, C. H.; Qiao, S. Z.; Zou, J.; Liu, G.; Smith, S. C.; Cheng, H. M.; Lu, G. Q. Anatase TiO_2 Single Crystals with a Large Percentage of Reactive Facets. *Nature* **2008**, *453*, 638−641.
(25) Gould, I. The Antibiotic Paradox. In *Antibiotic Policies*; Gould, I. M., Meer, J. W. M., Eds.; Springer: New York, 2012; pp 15−25.
(26) Golet, E. M.; Alder, A. C.; Giger, W. Environmental Exposure and Risk Assessment of Fluoroquinolone Antibacterial Agents in Wastewater and River Water of the Glatt Valley Watershed, Switzerland. *Environ. Sci. Technol.* **2002**, *36*, 3645−3651.
(27) Miao, X. S.; Bishay, F.; Chen, M.; Metcalfe, C. D. Occurrence of Antimicrobials in the Final Effluents of Wastewater Treatment Plants in Canada. *Environ. Sci. Technol.* **2004**, *38*, 3533−3541.
(28) Kanakaraju, D.; Glass, B.; Oelgemöller, M. Titanium Dioxide Photocatalysis for Pharmaceutical WasteWater Treatment. *Environ. Chem. Lett.* **2014**, *12*, 27−47.
(29) Van Doorslaer, X.; Heynderickx, P. M.; Demeestere, K.; Debevere, K.; Van Langenhove, H.; Dewulf. TiO_2 Mediated Heterogeneous Photocatalytic Degradation of Moxifloxacin: Operational Variables and Scavenger Study. *J. Appl. Catal. B: Environ.* **2012**, *111−112*, 150−156.
(30) Wang, J.; Dai, J.; Meng, M.; Song, Z.; Pan, J.; Yan, Y.; Li, C. Surface Molecularly Imprinted Polymers Based on Yeast Prepared by Atom Transfer Radical emulsion Polymerization for Selective Recognition of Ciprofloxacin from Aqueous Medium. *J. Appl. Polym. Sci.* **2014**, *131*, 40310(1−10).
(31) Kitano, M.; Wada, E.; Nakajima, K.; Hayashi, S.; Miyazaki, S.; Kobayashi, H.; Hara, M. Protonated Titanate Nanotubes with Lewis and Brønsted Acidity: Relationship between Nanotube Structure and Catalytic Activity. *Chem. Mater.* **2013**, *25*, 385−393.
(32) Lin, C.-H.; Wong, D. S. H.; Lu, S.-Y. Layered Protonated Titanate Nanosheets Synthesized with a Simple One-Step, Low Temperature, Urea-Modulated Method as an Effective Pollutant Adsorbent. *ACS Appl. Mater. Interfaces* **2014**, DOI: 10.1021/am5035335.
(33) Wada, E.; Kitano, M.; Nakajima, K.; Hara, M. Effect of Preparation Conditions on the Structural and Acid Catalytic Properties of Protonated Titanate Nanotubes. *J. Mater. Chem. A* **2013**, *1*, 12768−12774.
(34) Zhang, H.; Cao, L.; Liu, W.; Su, G. A New Ion Exchange Behavior of Protonated Titanate Nanotubes after Deprotonation and the Study on Their Morphology and Optical Properties. *Appl. Surf. Sci.* **2012**, *259*, 610−615.
(35) Yang, X. F.; Karthik, C.; Li, X. Y.; Fu, J. X.; Fu, X. H.; Liang, C. L.; Ravishankar, N.; Wu, M. M.; Ramanath, G. Oriented Nanocrystal Arrays of Selectable Polymorphs by Chemical Sculpture. *Chem. Mater.* **2009**, *21*, 3197−3201.
(36) An, T.; Yang, H.; Li, G.; Song, W.; Cooper, W. J.; Nie, X. Kinetics and Mechanism of Advanced Oxidation Processes (AOPs) in Degradation of Ciprofloxacin in Water. *Appl. Catal., B* **2010**, *94*, 288−294.
(37) Sutradhar, N.; Pahari, S. K.; Jayachandran, M.; Stephan, A. M.; Nair, J. R.; Subramanian, B.; Bajaj, H. C.; Mody, H. M.; Panda, A. B. Organic Free Low Temperature Direct Synthesis of Hierarchical Protonated Layered Titanates/Anatase TiO_2 Hollow Spheres and Their Task-Specific Applications. *J. Mater. Chem. A* **2013**, *1*, 9122−9131.
(38) Feng, Q.; Hirasawa, M.; Yanagisawa, K. Synthesis of Crystal-Axis-Oriented $BaTiO_3$ and Anatase Platelike Particles by a Hydrothermal Soft Chemical Process. *Chem. Mater.* **2001**, *13*, 290−296.
(39) Wen, P.; Itoh, H.; Tang, W.; Feng, Q. Single Nanocrystals of Anatase-Type TiO2 Prepared from Layered Titanate Nanosheets: Formation Mechanism and Characterization of Surface Properties. *Langmuir* **2007**, *23*, 11782−11790.
(40) Chen, Q.; Mogilevsky, G.; Wagner, G. W.; Forstater, J.; Kleinhammes, A.; Wu, Y. Active Anatase (0 0 1)-Like Surface of

Hydrothermally Synthesized Titania Nanotubes. *Chem. Phys. Lett.* **2010**, *485*, 262−262.
(41) Mogilevsky, G.; Chen, Q.; Kulkarni, H.; Kleinhammes, A.; Mullins, W. M.; Wu, Y. Layered Nanostructures of Delaminated Anatase: Nanosheets and Nanotubes. *J. Phys. Chem. C* **2008**, *112*, 3239−3246.
(42) Du, R.; Su, R.; Li, X.; Tantai, X.; Liu, Z.; Yang, J.; Qi, W.; He, Z. Controlled Adsorption of Cellulase onto Pretreated Corncob by pH Adjustment. *Cellulose* **2012**, *19*, 371−380.
(43) Fukahori, S.; Fujiwara, T.; Ito, R.; Funamizu, N. pH-Dependent Adsorption of Sulfa Drugs on High Silica Zeolite: Modeling and Kinetic Study. *Desalination* **2011**, *275*, 237−242.
(44) Paszko, T. Effect of pH on the Adsorption of Carbendazim in Polish Mineral Soils. *Sci. Total Environ.* **2012**, *435*−*436*, 222−229.
(45) Luis Vázquez, J.; Berlanga, M.; Merino, S.; Domènech, Ò.; Viñas, M.; Teresa Montero, M.; Hernández-Borrell, J. Determination by Fluorimetric Titration of the Ionization Constants of Ciprofloxacin in Solution and in the Presence of Liposomes. *Photochem. Photobiol.* **2001**, *73*, 14−19.
(46) Carrasquillo, A. J.; Bruland, G. L.; MacKay, A. A.; Vasudevan, D. Sorption of Ciprofloxacin and Oxytetracycline Zwitterions to Soils and Soil Minerals: Influence of Compound Structure. *Environ. Sci. Technol.* **2008**, *42*, 7634−7642.
(47) Sasaki, T.; Watanabe, M. Osmotic Swelling to Exfoliation. Exceptionally High Degrees of Hydration of a Layered Titanate. *J. Am. Chem. Soc.* **1998**, *120*, 4682−4689.
(48) Turel, I.; Golobic, A. Crystal Structure of Ciprofloxacin Hydrochloride 1.34-Hydrate. *Anal. Sci.* **2003**, *19*, 329−330.
(49) Fau, C. J. M. M.; Martìnez, A. J.; Cosme, G. A.; Villasante, P. J. Crystalline Form of Moxifloxacin Base. Google Patents EP 2154137 A1, 2010.
(50) Huber, C. P.; Sake Gowda, D. S.; Ravindra Acharya, K. Refinement of the Structure of Nalidixic Acid. *Acta Crystallogr. B* **1980**, *36*, 497−499.
(51) Qian, J.-J.; Gu, J.-M.; Shen, J.; Hu, X.-R.; Wu, S.-X. Moxifloxacinium Chloride Monohydrate. *Acta Crystallogr. E* **2011**, *67*, o2773−o2774.
(52) Zhang, S.; Peng, L. M.; Chen, Q.; Du, G. H.; Dawson, G.; Zhou, W. Z. Formation Mechanism of $H_2Ti_3O_7$ Nanotubes. *Phys. Rev. Lett.* **2003**, *91*, 256103.
(53) Yamaguchi, K.; Tamura, Z.; Maeda, M. Molecular Structure of the Zwitterionic Form of Phenolsulfonphthalein. *Anal. Sci.* **1997**, *13*, 521−522.
(54) Zhang, Z.; Wang, P. Optimization of Photoelectrochemical Water Splitting Performance on Hierarchical TiO_2 Nanotube Arrays. *Energy Environ. Sci.* **2012**, *5*, 6506−6512.
(55) Wood, D. L.; Tauc, J. Weak Absorption Tails in Amorphous Semiconductors. *Phys. Rev. B* **1972**, *5*, 3144−3151.
(56) Gong, X.-Q.; Selloni, A. Reactivity of Anatase TiO_2 Nanoparticles: The Role of the Minority (001) Surface. *J. Phys. Chem. B* **2005**, *109*, 19560−19562.
(57) Vittadini, A.; Selloni, A.; Rotzinger, F. P.; Grätzel, M. Structure and Energetics of Water Adsorbed at TiO_2 Anatase 101 and 001 Surfaces. *Phys. Rev. Lett.* **1998**, *81*, 2954−2957.
(58) Fang, W. Q.; Gong, X. Q.; Yang, H. G. On the Unusual Properties of Anatase TiO_2 Exposed by Highly Reactive Facets. *J. Phys. Chem. Lett.* **2011**, *2*, 725−734.
(59) Diebold, U. The Surface Science of Titanium Dioxide. *Surf. Sci. Rep.* **2003**, *48*, 53−229.
(60) An, T.; Chen, J.; Li, G.; Ding, X.; Sheng, G.; Fu, J.; Mai, B.; O'Shea, K. E. Characterization and the Photocatalytic Activity of TiO_2 Immobilized Hydrophobic Montmorillonite Photocatalysts: Degradation of Decabromodiphenyl Ether (BDE 209). *Catal. Today* **2008**, *139*, 69−76.
(61) Chen, J.; Li, G.; He, Z.; An, T. Adsorption and Degradation of Model Volatile Organic Compounds by a Combined Titania−Montmorillonite−Silica Photocatalyst. *J. Hazard. Mater.* **2011**, *190*, 416−423.